Phase retrieval from angular streaking of XUV atomic ionization

Anatoli S. Kheifets[1], Kyung Taec Kim[2,3], Igor A. Ivanov[2], Anna Li Wang[4], and James P. Cryan[4]
[1]*Research School of Physics, The Australian National University, Canberra ACT 2601, Australia**
[2]*Center for Relativistic Laser Science, Institute for Basic Science, Gwangju 61005, Korea*
[3]*Department of Physics and Photon Science, GIST, Gwangju 61005, Korea and*
[4]*Stanford PULSE Institute SLAC National Accelerator Laboratory, USA*
(Dated: January 5, 2022)

We demonstrate an accurate phase retrieval of XUV atomic ionization by streaking the photoelectron in a circularly polarized IR laser field. The streaking phase can then be converted to the atomic time delay containing the Wigner and continuum-continuum components. Our demonstration is based on a numerical solution of the time-dependent Schrödinger equation. We test this technique using the hydrogen atom ionized by an isolated attosecond XUV pulse spanning a wide range of photon energies. Comparison with predictions of the lowest order perturbation theory validates our technique and makes it applicable to a broad range of atomic and molecular targets. Validity and implications of the strong field approximation are also discussed.

PACS numbers: 32.80.Rm 32.80.Fb 42.50.Hz

Angular streaking of XUV atomic ionization with a circularly polarized IR laser radiation has become a useful tool for characterizing isloated attosecond pulses (IAP) from free-electron laser (FEL) sources. First suggested theoretically [1–3], this method has been implemented in practice for a shot-to-shot characterization of IAP at FEL [4, 5]. Angular streaking of XUV ionization combines elements of the two previously developed techniques: attosecond angular streaking known as the attoclock [6–8] and the attosecond streak camera [9–16]. It is analogous to the attosecond streak camera by using XUV primary ionization while it is similar to the attoclock by steering the ionized electron with a circularly polarized laser radiation and detecting the photoelectron in the polarization plane. The difference with the attoclock is that the latter is a self-referencing technique where both tunneling ionization and steering are produced by the same elliptical IR laser pulse. In its original form [1–5], angular streaking of XUV ionization was considered in an intense IR laser field which induced large photoelectron momentum shifts. This allowed to analyze this process within the strong field approximation (SFA). In the meantime, the onset of streaking at significantly weaker IR fields can be interpreted within the lowest order perturbation theory (LOPT) [17–19]. Under such conditions, IR streaking can be considered as an interference phenomenon which opens a natural access to the streaking phase Φ_s. The latter contains the XUV ionization phase (the Wigner phase) and the continuum-continuum phase from the IR interaction. These two phases can be converted to the corresponding time delay components which add up to the atomic time delay. This delay can be interpreted as the time it takes for the electron to be photoionized plus the time it takes for the measurement process to occur. This timing analysis has been used to determine the attosecond time delay in photoemission from atoms [20] and solid surfaces [21]. The latter seminal papers opened up the rapidly growing field of attosecond chronoscopy of photoemission [22–24]. While the angular streaking of XUV ionization is conceptually similar to the analogous process utilizing linear streaking, its phase retrieval capability has not been explored so far. There has been a suggestion to retrieve the XUV ionization phase in a strong field regime using the SFA [25]. However, such a technique would only be applicable to energetic photoelectrons which carry typically a rather small Wigner phase and the corresponding time delay. Much more interesting XUV ionization processes, which are strongly affected by many-electron correlation, would not be accessible by this technique.

In this Letter, we propose an alternative phase retrieval method which is applicable in a very wide range of photoelectron energies right from the ionization threshold. We demonstrate the accuracy of this technique by considering the hydrogen atom driven by an attosecond XUV pulse in a wide range of carrier frequencies. Our demonstration is based on a numerical solution of the time-dependent Schrödinger equation (TDSE), and is validated through comparison with the LOPT predictions. The technique is applicable to a broad range of atomic and molecular targets. At the same time, we test the validity of the SFA which offers an alternative phase retrieval method. Surprisingly, the two complementary techniques produce very similar results.

An interference character of IR streaking of XUV ionization is illustrated in the left panel of Fig. 1. There are three ionization channels marked (d), (a) and (e) leading to the same final state with the photoelectron energy E. While the direct channel (d) contains an unassisted XUV ionization, two other channels are aided by an IR absorption (a) or emission (e). For these three channels to interfere, the spectral width of the XUV pulse should be large enough to accommodate the $\pm\omega$ processes. Such a spectrum is illustrated in the right panel of Fig. 1

*Electronic address: A.Kheifets@anu.edu.au

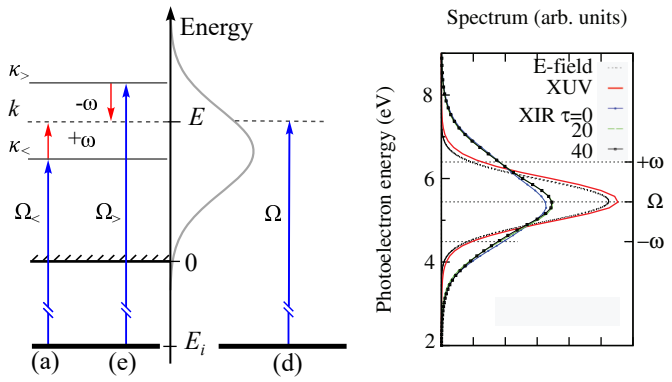

FIG. 1: Left: Schematic representation of IR streaking of XUV ionization. The first order direct process (d) and the second order processes aided by an IR photon absorption (a) and emission (d) are labeled accordingly (adopted from [18]). Right: photoelectron spectrum of H driven by XUV and XIR fields is overlapped with the E-field Fourier transform.

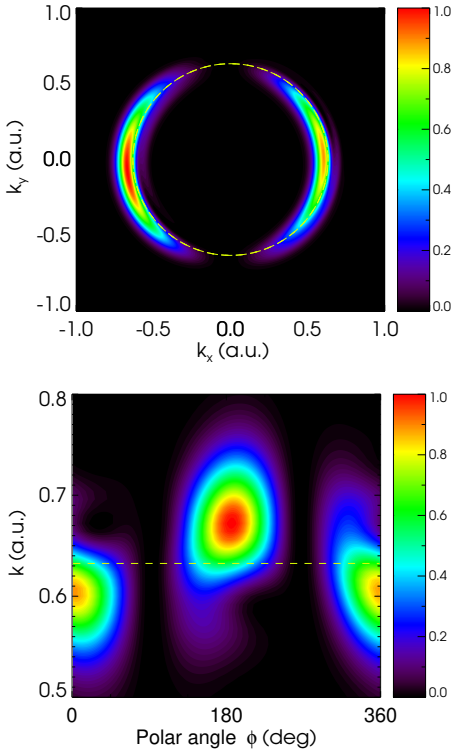

FIG. 2: The XUV+IR PMD of the hydrogen atom in the polarization plane displayed in the Cartesian (top) and polar (bottom) coordinates. The circle (top) and the straight line (bottom) highlight the momentum value $k_0 = \sqrt{2(\Omega - I_p)}$ from the energy conservation.

which corresponds to ionization of the hydrogen atom at the XUV and IR photon energies $\Omega = 0.7$ au and $\omega = 0.035$ au, respectively while the XUV pulse duration is restricted to 250 as. The photoelectron spectrum of an unassisted XUV photoionization (process d) is an exact replica of the Fourier transform of the electric field shifted by the ionization potential. Meanwhile, the photoelectron spectrum of XUV+IR ionization (XIR for brevity) is significantly broadened by the second-order (a) and (e) processes. The left panel of Fig. 1 illustrates the process in which the IR streaking leads to a net increase of the photoelectron energy $E > E_0$ where $E_0 = \Omega - I_p$ corresponds to the center of the photoelectron spectrum. An analogous process with $E < E_0$ can be exhibited in a similar way.

Fig. 2 displays the photoelectron momentum distribution (PMD) of the hydrogen atom ionized with a 250 as XUV pulse at 1.5×10^{15} W/cm^2 and $\Omega = 0.7$ au which is streaked with a long IR pulse with $\omega = 0.035$ au ($\lambda = 1030$ nm) at 1.5×10^{11} W/cm^2 . The XUV pulse is linearly polarized along the $\hat{x}$ axis whereas the IR pulse is circularly polarized in the (xy) plane. The PMD is projected on this plane. The top panel illustrates the dipole angular pattern $\propto \cos^2\phi$ of the primary XUV ionization of the hydrogen $1s$ initial state which is largely retained in the XIR process. The bottom panel shows the polar coordinate representation of the PMD, highlighting the momentum offset induced by the vector potential $A_{\rm IR} = 0.06$ au.

The PMD exhibited in Fig. 2 was obtained using the TDSE simulation with the spherical-coordinate implicit derivatives (SCID) computer code [26]. The code was cross-checked against another numerical TDSE implementation [27] and both methods produced nearly identical results. A typical calculation involved 10 partial waves and was propagated over 50 fs on a radial grid of 360 Bohr. Such a calculation would normally take about 40 CPU hours on a massively parallel system ranked in the top 50 of the commercially available computer systems [28]. In the present implementation, the Volkov Hamiltonian was used to propagate TDSE in the asymptotic region which allowed to save computational time by employing a smaller radial grid. At each XUV photon frequency, we run a series of calculations with a fixed delay $\tau = n\Delta\tau$ between the centers of the XUV and IR pulses with $0 \le n \le 6$ and the increment $\Delta\tau = 10$ au.

To highlight the angular streaking effect, we integrate the PMD illustrated in Fig. 2 over the radial momentum and produce the angular profile $P(\phi)$, where the polar angle ϕ in the (x, y) plane is counted from the $\hat{x}$ axis aligned with the linear polarization direction of the XUV pulse. To display more clearly the interference effect, we subtract the unassisted XUV profile from those obtained in both XUV and IR fields. The differential angular profiles $P_{\rm XIR}(\phi, \tau) - P_{\rm XUV}(\phi)$ at various XUV/IR delays τ are presented in the top panel of Fig. 3. This panel spans emission angles $90° < \phi < 270°$ and focuses on the PMD lobe in which the photoelectron linear momentum is streaked up. Similar series of curves can be produced for another lobe at $-90° < \phi < 90°$ in which the linear momentum is streaked down. In both cases, the differential angular profiles are regularly spaced as the XUV/IR

delay τ is incremented by $\Delta\tau$.

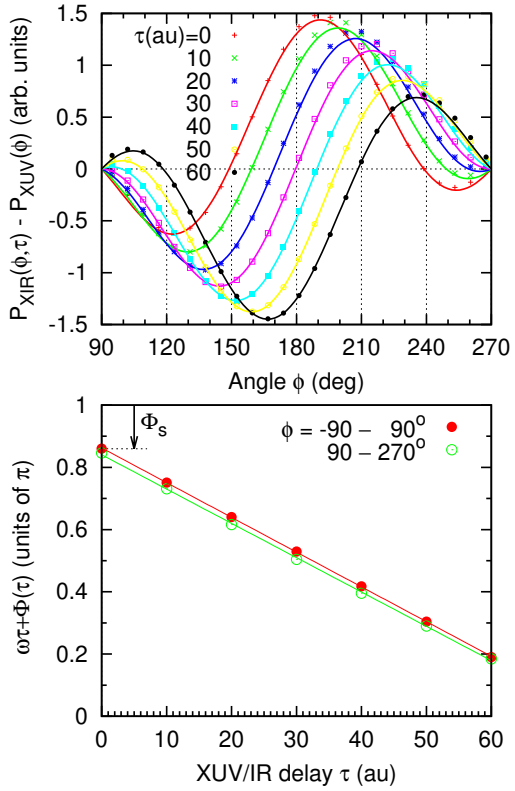

FIG. 3: Top: the differential angular profiles $P_{\rm XIR}(\phi,\tau) - P_{\rm XUV}(\phi)$ produced by the radial integration of the PMD of Fig. 2 at various XUV/IR delays τ. The dots visualize numerical TDSE results whereas the similarly colored solid lines represent the fit with Eq. (3). Bottom: Streaking phase extraction from fitting the differential angular profiles with Eq. (3).

To interpret this angular displacement effect, we adopt the LOPT formalism [18]. We align the quantization $\hat{z}$ axis with the joint propagation direction of both laser pulses. In this frame, the linearly polarized XUV pulse can be represented as a superposition of the two circularly polarized pulses with the opposite helicities. Hence the angular dependence of the XUV ionization amplitude in the (x,y) plane ($\theta=\pi/2$) can be written as

$$\mathcal{M}_{\rm XUV}(\boldsymbol{k}) \propto Y_{1-1}(\hat{\boldsymbol{k}}) - Y_{11}(\hat{\boldsymbol{k}}) \propto e^{i\phi} + e^{-i\phi} \propto \cos\phi \quad (1)$$

Subsequent absorption or emission of the circularly polarized IR photon would add or subtract one unit of the angular momentum projection. This would lead to the final $M=0,2$ projections. We ignore the zero projection which carries no ϕ dependence and present the XIR amplitude as

$$\mathcal{M}_{\rm XIR}(\boldsymbol{k}) \propto Y_{22}(\hat{\boldsymbol{k}}) e^{-i\omega\tau} \quad (2)$$

The interference term of the XUV and XIR amplitudes, which is responsible for the angular streaking, takes the form

$$\mathrm{Re}\Big[\mathcal{M}^*_{\rm XUV}(\boldsymbol{k})\mathcal{M}_{\rm XIR}(\boldsymbol{k})e^{-i\omega\tau}\Big] \propto \cos(2\phi-\omega\tau-\Phi_s+\pi)\cos\phi \quad (3)$$

Here we introduced the streaking phase Φ_s which is defined by an expression similar to Eq. (50) of [18]:

$$\begin{aligned}\Phi_s &= \arg\{\mathcal{M}^*_{\rm XUV}\mathcal{M}_{\rm XIR}\}+\pi \\ &\approx \phi_\Omega - \phi_{\Omega_<} + \eta_\lambda(k) - \eta_\lambda(\kappa_<) - \phi_{cc}(k,\kappa_<)\end{aligned} \quad (4)$$

Here $\kappa_< < k < \kappa_>$ are the photoelectron momenta marked in the left panel of Fig. 1 and the angular momentum $\lambda=1$ in the case of the hydrogen $1s$ state.

In our simulation we use a symmetric XUV pulse with a real Fourier transform $\int_{-\infty}^{\infty} dt\mathcal{E}(t)\sin\Omega t = 0$. So we can neglect the XUV phase difference in Eq. (4). Then we convert the XUV ionization phase difference into the Wigner time delay $\tau_{\rm W} = [\eta_\lambda(k) - \eta_\lambda(\kappa_<)]/\omega$ and introduce the CC time delay $\tau_{cc} = \phi_{cc}(k,\kappa_<)/\omega$. This way the streaking phase can be expressed via the atomic time delay as

$$\Phi_s = \omega(\tau_{\rm W}+\tau_{cc}) \equiv \omega\tau_a \quad (5)$$

To retrieve the streaking phase from our TDSE simulations, we fit the differential angular profiles of Fig. 2 with an ansatz of Eq. (3) using Φ_s as an adjustable parameter. The fitting results are shown in the bottom panel of Fig. 3. The two series of data in this figure visualize the fit of the two PMD lobes exhibited in the bottom panel of Fig. 2. The solid lines visualize the $\omega\tau$ slope while the intercept of these lines with $\tau=0$ axis corresponds to the streaking phase Φ_s. The procedure of the streaking phase extraction was carried out at a number of XUV photon energies and the resulting phase and the atomic time delay are shown in Fig. 5.

A complementary method of the streaking phase extraction can be derived from the SFA, following the method in reference [1]. The stationary phase principle connects the photoelectron momentum at the detector with the vector potential at the instant of ionization $t_{\rm st}$:

$$\Phi'(t_{\rm st}) = \frac{1}{2}|\boldsymbol{k} - \boldsymbol{A}_L(t_{\rm st})|^2 - E_0 = 0 \quad (6)$$

We assume the XUV pulse is short and shifted relative to the peak of the IR pulse by the time τ. This leads to the following *isochrone* equation [1]:

$$k^2/2 - E_0 = kA_0\cos(\phi-\omega\tau)\,; \quad \begin{cases} k>k_0 & \phi-\omega\tau=0 \\ k<k_0 & \phi-\omega\tau=180^\circ \end{cases}$$

The isochrone curve is visible in the polar coordinate representation of the PMD in the bottom panel of Fig. 2, which has XIR delay $\tau=0$. Other τ cases are illustrated below in the top panel of Fig. 4.

We can modify this isochrone equation using a complex-valued dipole matrix element with a linear energy dependent phase. We find that the dipole matrix

element phase can be read directly from the isochrone phase offset, just like the XIR delay [33]:

$$k_{\pm}^2/2 - E_0 = \pm k A_0 \cos(\phi - \omega\tau - \Phi_s) \qquad (7)$$

To determine $k_{\pm}$, we integrate the PMD exhibited in Fig. 2 over the angular intervals encompassing the downwards (-) and upwards (+) shifted lobes which are centered at $\phi = 0$ and 180°, respectively. We carry this procedure at several fixed increments of the XUV/IR delay τ. The corresponding radial momentum profiles $P(k,\tau)$ are shown in the top panel of Fig. 4 for the angular integration range $-90° < \phi < 90°$ corresponding to the k_- solution. The analogous profiles corresponding to the k_+ solution mirror closely that of the k_- one. The centers of the momentum profiles $P(k,\tau)$ are fitted with a Gaussian function and thus determined peak positions $k_{\pm}$ are plotted on the bottom panel of Fig. 4. Here we fit the radial momentum displacements $k_{\pm}^2 - E_0$ with the isochrone ansatz (7) to determine Φ_s.

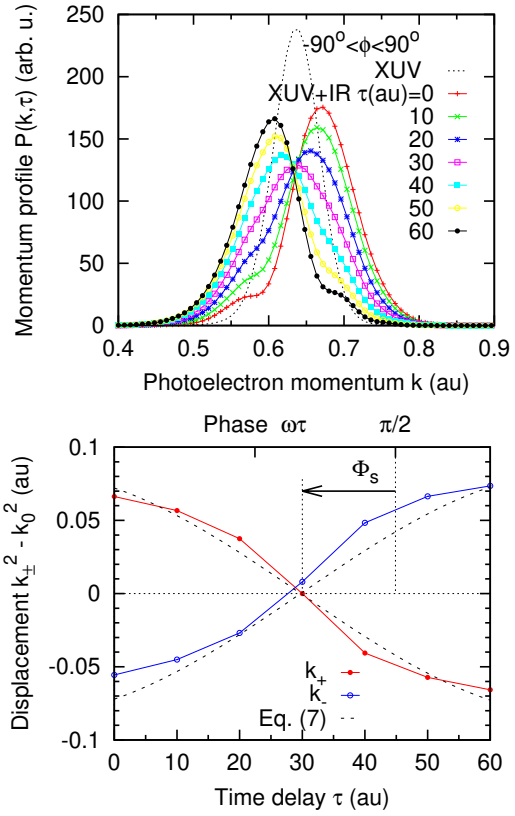

FIG. 4: Top: radial momentum profiles after angular integration in the $-90° < \phi < 90°$ range. The peaks of $P(k,\tau)$ define the shifted photoelectron momentum k_-. Bottom: radial momentum displacements $k_{\pm}^2/2 - k_0^2/2$ are shown at various XUV/IR delays τ. The dashed line represents the fit with Eq. (7).

In Fig. 5 we compare the streaking phase Φ_s extracted by the two methods utilizing the angular ansatz of Eq. (3) and the radial ansatz of Eq. (7). The left vertical axis displays Φ_s in radians while the right axis is calibrated in units of the time delay with Eq. (5) conversion. We use the latter axis to overplot the expected atomic time

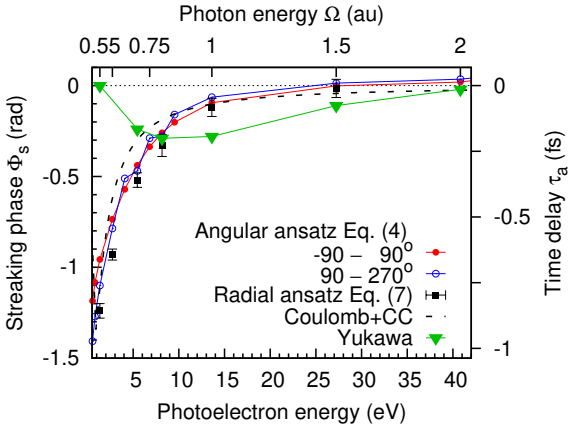

FIG. 5: Streaking phase Φ_s (left vertical axis) and the atomic time delay τ_a (right axis) extracted using the angular Eq. (3) and radial Eq. (7) anstatzen. The time delay axis is used to display the sum of the Coulomb time delay and the CC correction.

delay $\tau_a = \tau_W + \tau_{cc}$. As the hydrogen atom is free from many-electron correlation, the Wigner time delay τ_W is calculated from the Coulomb elastic scattering phase in the partial p-wave. The hydrogenic CC correction τ_{cc} is digitized and extrapolated from Fig. (9) of [18]. We observe in Fig. 5 a good agreement between the streaking phase values retrieved by the two complementary extraction methods and a close correspondence with the hydrogenic time delay. In addition, we run a set of similar simulations with the Yukawa atom in which the Coulomb potential is screened as $(Z/r)\exp(-r/a)$, where $Z = 2.785$ and $a = 0.5$ thus maintaining the hydrogen atom ionization potential. XUV ionization is initiated at a distance k^{-1}. So the Coulomb potential is screened efficiently for slow photoelectrons electrons with $k < 1$. As the result, the streaking phase gradually vanishes towards the ionization potential while approaching that of the hydrogen atom for fast photoelectrons.

In conclusion, we demonstrate an accurate retrieval of the streaking phase Φ_s from XUV atomic ionization in the presence of a circularly polarized IR laser field. We introduce two complementary techniques that allow us to extract Φ_s from the radial and angular displacement of the photoelectron momentum distribution projected on the plane of the circular polarization. Both methods produce very similar results which compare closely with predictions of the lowest order perturbation theory. The LOPT interpretation allows us to connect Φ_s with the atomic time delay τ_a [34] which contains the time it takes for the electron to be photoionized and the time it takes for the measurement process. This interpretation was questioned recently for the Coulombic systems [29] but seems to be confirmed by the present study. The proposed method has a wide range of applicability spanning the photoelectron energies from threshold to several ionization potentials.

The proposed phase retrieval from angular streaking

of XUV ionization can be used in measurements from XFEL sources, which give access to ionization from the inner atomic shells. Small adjustments to the method need to be made for experimental realization, particularly to compensate for the stochastic timing jitter of the XFEL pulses. This has been accomplished by using a reference photoline to remove the pump/probe time delay (τ). Rather than measuring the absolute streaking angle, one can measure the relative streaking angles between the target photoline and the reference photoline, which share some common global streaking angle due to τ [30]. Energy resolved spin-orbit doublets are convenient targets with built-in referencing, allowing inherent subtraction of the streaking contributions from τ, XUV pulse phase, and continuum-continuum coupling. Such accurate determination of the Wigner phase and time delay will shed new light on correlation induced attosecond ionization dynamics. As the prime candidate for such a measurement, the $3d$ ionization of the Xe atom is considered where the spin-split $3d_{3/2,5/2}$ components display a strong correlation induced modification of the photoionization cross-section and angular anisotropy βparameter [31]. To account for this process, electron correlation driven channel-coupling effects between the spin-orbit split channels must be included [32]. The preparation for this measurement is currently underway.

Serguei Patchkovskii is acknowledged for placing his iSURF TDSE code at our disposal. Resources of National Computational Infrastructure facility (NCI Australia) have been employed.

[1] A. K. Kazansky, A. V. Bozhevolnov, I. P. Sazhina, and N. M. Kabachnik, *Interference effects in angular streaking with a rotating terahertz field*, Phys. Rev. A **93**, 013407 (2016).

[2] S. Li, Z. Guo, R. N. Coffee, K. Hegazy, Z. Huang, A. Natan, T. Osipov, D. Ray, A. Marinelli, and J. P. Cryan, *Characterizing isolated attosecond pulses with angular streaking*, Opt. Express **26**(4), 4531 (2018).

[3] A. K. Kazansky, I. P. Sazhina, and N. M. Kabachnik, *Fast retrieval of temporal characteristics of fel pulses using streaking by thz field*, Opt. Express **27**(9), 12939 (2019).

[4] N. Hartmann, G. Hartmann, R. Heider, M. S. Wagner, M. Ilchen, J. Buck, A. O. Lindahl, C. Benko, J. Grünert, J. Krzywinski, et al., *Attosecond time-energy structure of x-ray free-electron laser pulses*, Nature Photonics **12**, 215 (2018).

[5] J. Duris, S. Li, T. Driver, E. G. Champenois, J. P. MacArthur, A. A. Lutman, Z. Zhang, P. Rosenberger, J. W. Aldrich, R. Coffee, et al., *Tunable isolated attosecond x-ray pulses with gigawatt peak power from a free-electron laser*, Nature Photonics **14**, 30 (2020).

[6] P. Eckle, M. Smolarski, P. Schlup, J. Biegert, A. Staudte, M. Schoffler, H. G. Muller, R. Dorner, and U. Keller, *Attosecond angular streaking*, Nat. Phys. **4**, 565 (2008).

[7] P. Eckle, M. Smolarski, P. Schlup, J. Biegert, A. Staudte, M. Schoffler, H. G. Muller, R. Dorner, and U. Keller, *Attosecond angular streaking*, Nat Phys **4**, 565 (2008).

[8] A. N. Pfeiffer, C. Cirelli, M. Smolarski, D. Dimitrovski, M. Abu-samha, L. B. Madsen, and U. Keller, *Attoclock reveals natural coordinates of the laser-induced tunnelling current flow in atoms*, Nat Phys **8**, 76 (2012).

[9] E. Constant, V. D. Taranukhin, A. Stolow, and P. B. Corkum, *Methods for the measurement of the duration of high-harmonic pulses*, Phys. Rev. A **56**, 3870 (1997).

[10] J. Itatani, F. Quéré, G. L. Yudin, M. Y. Ivanov, F. Krausz, and P. B. Corkum, *Attosecond streak camera*, Phys. Rev. Lett. **88**, 173903 (2002).

[11] E. Goulielmakis, M. Uiberacker, R. Kienberger, A. Baltuska, V. Yakovlev, A. Scrinzi, T. Westerwalbesloh, U. Kleineberg, U. Heinzmann, M. Drescher, et al., *Direct measurement of light waves*, Science **305**(5688), 1267 (2004).

[12] R. Kienberger, E. Goulielmakis, M. Uiberacker, A. Baltuska, V. Yakovlev, F. Bammer, A. Scrinzi, T. Westerwalbesloh, U. Kleineberg, U. Heinzmann, et al., *Atomic transient recorder*, Nature **427**, 817 (2004).

[13] V. S. Yakovlev, F. Bammer, and A. Scrinzi, *Attosecond streaking measurements*, J. Mod. Opt. **52**(2-3), 395 (2005).

[14] U. Frühling, M. Wieland, M. Gensch, T. Gebert, B. Schütte, M. Krikunova, R. Kalms, F. Budzyn, O. Grimm, J. Rossbach, et al., *Single-shot terahertz-field-driven x-ray streak camera*, Nature Photonics **3**, 523 (2009).

[15] C.-H. Zhang and U. Thumm, *Streaking and Wigner time delays in photoemission from atoms and surfaces*, Phys. Rev. A **84**, 033401 (2011).

[16] M. Ivanov and O. Smirnova, *How accurate is the attosecond streak camera?*, Phys. Rev. Lett. **107**, 213605 (2011).

[17] J. M. Dahlström, A. L. Huillier, and A. Maquet, *Introduction to attosecond delays in photoionization*, J. Phys. B **45**(18), 183001 (2012).

[18] J. M. Dahlström *et al*, *Theory of attosecond delays in laser-assisted photoionization*, Chem. Phys. **414**, 53 (2013).

[19] A. Maquet, J. Caillat, and R. Taeb, *Attosecond delays in photoionization: time and quantum mechanics*, J. Phys. B **47**(20), 204004 (2014).

[20] M. Schultze, M. Fiess, N. Karpowicz, J. Gagnon, M. Korbman, M. Hofstetter, S. Neppl, A. L. Cavalieri, Y. Komninos, T. Mercouris, et al., *Delay in Photoemission*, Science **328**(5986), 1658 (2010).

[21] A. L. Cavalieri, N. Müller, T. Uphues, V. S. Yakovlev, A. Baltuska, B. Horvath, B. Schmidt, L. Blümel, R. Holzwarth, S. Hendel, et al., *Attosecond spectroscopy in condensed matter*, Nature **449**, 1029 (2007).

[22] R. Pazourek, S. Nagele, and J. Burgdorfer, *Time-resolved photoemission on the attosecond scale: opportunities and challenges*, Faraday Discuss. **163**, 353 (2013).

[23] R. Pazourek, S. Nagele, and J. Burgdörfer, *Attosecond chronoscopy of photoemission*, Rev. Mod. Phys. **87**, 765 (2015).

[24] U. Thumm, Q. Liao, E. M. Bothschafter, F. Smann, M. F. Kling, and R. Kienberger, in *Photonics* (John Wiley & Sons, Ltd, 2015), chap. 13, pp. 387–441, ISBN 9781119009719, URL `https://onlinelibrary.wiley.`

com/doi/abs/10.1002/9781119009719.ch13.

[25] X. Zhao, H. Wei, W.-W. Yu, and C. D. Lin, *Reconstruction of the complex angle-dependent photoionization transition dipole from a laser-dressed streaking experiment*, Phys. Rev. A **98**, 053404 (2018).

[26] S. Patchkovskii and H. Muller, *Simple, accurate, and efficient implementation of 1-electron atomic time-dependent schrödinger equation in spherical coordinates*, Computer Physics Communications **199**, 153 (2016).

[27] I. A. Ivanov, *Evolution of the transverse photoelectron-momentum distribution for atomic ionization driven by a laser pulse with varying ellipticity*, Phys. Rev. A **90**, 013418 (2014).

[28] *The 500 Most Powerful Commercially Available Computer Systems*, Web (2021), URL https://www.top500.org/lists/top500/2021/06//.

[29] U. Saalmann and J. M. Rost, *Proper time delays measured by optical streaking*, Phys. Rev. Lett. **125**, 113202 (2020).

[30] T. D. Driver *et al*, *Isolated, tunable soft x-ray attosecond pulses at μj pulse energy from a free-electron laser*, in *7th International Conference on Attosecond Science and Technology* (University of Szeged, Hungary, 2019), URL https://www.eli-alps.hu/indico/event/22/timetable/?print=1&view=standard.

[31] A. Kivimäki, U. Hergenhahn, B. Kempgens, R. Hentges, M. N. Piancastelli, K. Maier, A. Rüdel, J. J. Tulkki, and A. M. Bradshaw, *Near-threshold study of xe 3d photoionization*, Phys. Rev. A **63**, 012716 (2000).

[32] V. Radojević, D. M. Davidović, and M. Y. Amusia, *Near-threshold photoionization of the xe 3d spin-orbit doublet: Relativistic, relaxation, and intershell interaction effects*, Phys. Rev. A **67**, 022719 (2003).

[33] See Supplementary Material for more information

[34] We can also connect Φ_s to the electron wave packet group delay using SFA, shown in the Supplementary Material.

Supplement to "Phase retrieval from angular streaking of XUV atomic ionization"

Anatoli S. Kheifets[1], Kyung Taec Kim[2,3], Igor A. Ivanov[2], Anna Li Wang[4], and James P. Cryan[4]
[1]*Research School of Physics, The Australian National University, Canberra ACT 2601, Australia*
[2]*Center for Relativistic Laser Science, Institute for Basic Science, Gwangju 61005, Korea*
[3]*Department of Physics and Photon Science, GIST, Gwangju 61005, Korea and*
[4]*Stanford PULSE Institute SLAC National Accelerator Laboratory, USA*
(Dated: January 5, 2022)

I. EFFECT OF DIPOLE PHASE ON ELECTRON MOMENTUM DISTRIBUTION

It is not immediately obvious that the phase of the dipole matrix element is contained in the angular shift of the measured photoelectron momentum distribution. Others have previously shown that the delay between the XUV and IR fields can be directly read from the linearly polarized streaking trace [1] or circularly polarized streaking isochrone [2]. Here we extend these derivations to demonstrate that the dipole matrix element is equivalent to an electronic wavepacket (EWP) group delay, and can be directly mapped onto streaking angle using the angular streaking method.

A. Equivalence of Dipole Matrix Phase and Time Delay in Streaking

Electron streaking is a two-photon process where an electron is photoionized by a combined XUV and IR field. Streaking is typically considered in the Strong Field Approximation (SFA) - the electron is photoionized by the two color field in a dipole approximation and the free electron then propagates in the continuum under the influence of relatively strong IR field. The initial electron momentum is $\boldsymbol{p} - \boldsymbol{A}(t)$, where $\boldsymbol{p}$ is the excess momentum from above threshold ionization with the XUV field and $\boldsymbol{A}(t)$ is the instantaneous vector potential of the streaking field at the moment of ionization. The SFA probability amplitude of finding a electron of momentum $\boldsymbol{p} - \boldsymbol{A}(t)$ is given by:

$$b(\boldsymbol{p}, \tau) = i \int_{t_0}^{\infty} dt \boldsymbol{E}(t-\tau) \cdot \vec{d}\,(\boldsymbol{p} - \boldsymbol{A}(t))\, e^{-i\Phi(t)}, \tag{1}$$

where Φ is given by,

$$\Phi(t) = \int_{t}^{\infty} dt' \frac{1}{2} \left[\boldsymbol{p} - \boldsymbol{A}(t')\right]^2 - I_p t, \tag{2}$$

For angular streaking, we use a circularly polarized IR streaking field, given by:

$$\boldsymbol{A}(t) = A_0(t) \left[\hat{x} \cos(\omega t) + \hat{y} \sin(\omega t)\right]. \tag{3}$$

Expanding Eq. (2) yields

$$\begin{aligned} \Phi(t) \;=\; & \left[\frac{p^2}{2} + I_p\right](T - t) - I_p T + \int_{T}^{\infty} dt' \frac{p^2 + A^2}{2} + \cancelto{\sim 0}{\int_{t}^{T} \frac{|A|^2}{2}} \\ & - p_x \left(A_0(t) \int_{t}^{T_x} dt' \cos(\omega t') + \cancelto{0}{\int_{T_x}^{\infty} dt' A_0(t') \cos(\omega t')} \right) \\ & - p_y \left(A_0(t) \int_{t}^{T_y} dt' \sin(\omega t') + \cancelto{0}{\int_{T_y}^{\infty} dt' A_0(t') \sin(\omega t')} \right), \end{aligned} \tag{4}$$

where in the second an third lines we have assumed that the streaking laser field envelope is approximately constant over a single period of the field to bring the envelope term, $A_0(t)$, outside the intergral in the first term. We have also assumed that $|\boldsymbol{p}| \gg |\boldsymbol{A}_0|$ in neglecting the 4th term in the first line. Additionally we have defined the special times T_x and T_y where the electric field $\boldsymbol{E}_{IR}(t) = \partial \boldsymbol{A}(t)/\partial t$ is directed along the $x-$ or $y-$axis respectively:

$$\boldsymbol{A}(T_x) = A_0(T_x)\hat{y} \tag{5}$$

$$\boldsymbol{A}(T_y) = A_0(T_y)\hat{x} \tag{6}$$

It should be clear that $T_x = T_y + T/4$, where T is the period of the IR streaking field. Then we can rewrite Eq. (1) as

$$b(\boldsymbol{p},\tau) = ie^{-i\left[\int_T^\infty dt' \frac{p^2+A^2}{2} - I_p T\right]} \int_{t_0}^\infty dt \boldsymbol{E}(t-\tau)\cdot\hat{d}\,|d\,(\boldsymbol{p}-\boldsymbol{A}(t))|\, e^{-i\left[\frac{p^2}{2}+I_p\right](T-t)}$$
$$\times\exp\left\{iA_0(t)\left(p_x\int_t^{T_x} dt'\cos(\omega t') + p_y\int_t^{T_y} dt'\sin(\omega t')\right)\right\} \tag{7}$$

This expression demonstrates an interesting property of SFA for streaking experiments - the momentum shift of the electron is acquired in the first quarter cycle of propagation.

To illustrate how the dipole matrix element phase is equivalent to the EWP group delay, we write an example, complex-valued dipole matrix element as, $\vec{d}(\boldsymbol{p}) = \hat{d}\,|d(\boldsymbol{p})|\, e^{-i\alpha(\boldsymbol{p})\frac{p^2}{2}}$. This phase explicitly exhibits the lowest order, linear dependance of the matrix element on the electron energy, which we aim to measure in angular streaking. In what follows we will drop the momentum dependence of α. Then we need to consider the expression,

$$\vec{d}\,(\boldsymbol{p}-\boldsymbol{A}(t)) = |d\,(\boldsymbol{p}-\boldsymbol{A}(t))|\, e^{-i\alpha\frac{[\boldsymbol{p}-\boldsymbol{A}(t)]^2}{2}} \tag{8}$$
$$\sim |d\,(\boldsymbol{p}-\boldsymbol{A}(t))|\, e^{-i\alpha\frac{p^2}{2}} e^{i\alpha\boldsymbol{p}\cdot\boldsymbol{A}(t)}, \tag{9}$$

where again we use the approximation $|\boldsymbol{p}| \gg |\boldsymbol{A}_0|$ to write the last term. We can rewrite the $\boldsymbol{p}\cdot\boldsymbol{A}(t)$ term as

$$\boldsymbol{p}\cdot\boldsymbol{A}(t) = A_0(t)\left[p_x\cos(\omega t) + p_y\sin(\omega t)\right] \tag{10}$$
$$= A_0(t)\left[p_x\int_t^{T_x} dt'\omega\sin(\omega t') - p_y\int_t^{T_y} dt'\omega\cos(\omega t')\right] \tag{11}$$

In plugging Eq. (11) into Eq. (9) and then using this to further simplify Eq. (7) we will need the following expressions:

$$\int_t^{T_y} dt'\left(\sin(\omega t') - \alpha\omega\cos(\omega t')\right) = \sqrt{1+(\alpha\omega)^2}\int_t^{T_y} dt'\sin[\omega(t'-\tau_\alpha)] \tag{12}$$
$$= \sqrt{1+(\alpha\omega)^2}\left[\int_{t+\tau_\alpha}^{T_y} + \int_{T_y}^{T_y+\tau_\alpha}\right] dt'\sin(\omega t')$$
$$\int_t^{T_x} dt'\left(\cos(\omega t') + \alpha\omega\sin(\omega t')\right) = \sqrt{1+(\alpha\omega)^2}\int_t^{T_x} dt'\cos(\omega t'-\tau_\alpha) \tag{13}$$
$$= \sqrt{1+(\alpha\omega)^2}\left[\int_{t+\tau_\alpha}^{T_x} + \int_{T_x}^{T_x+\tau_\alpha}\right] dt'\cos(\omega t')\ ,$$

where $\tau_\alpha = \omega^{-1}\mathrm{atan}(\alpha\omega) \sim \alpha$. Then we can rewrite Eq. (7),

$$b(\boldsymbol{p},\tau) = ie^{-i\left[\int_T^\infty dt' \frac{p^2+A^2}{2} + I_p(T+\alpha)\right]} \int_{t_0}^\infty dt \boldsymbol{E}(t-\tau)\cdot\hat{d}\,|d\,(\boldsymbol{p}-\boldsymbol{A}(t))|\, e^{i\left[\frac{p^2}{2}+I_p\right](T-t-\alpha)}$$
$$\times\exp\left\{iA_0(t)\sqrt{1+(\alpha\omega)^2}\left(p_x\int_{t+\tau_\alpha}^{T_c} dt'\cos(\omega t') + p_y\int_{t+\tau_\alpha}^{T_s} dt'\sin(\omega t')\right)\right\}$$

Finally we make the substitution, $\bar{t} = t + \tau_\alpha$

$$b(\boldsymbol{p},\tau) = ie^{-i\left[\int_T^\infty dt' \frac{p^2+A^2}{2} + I_p(T+\alpha)\right]} \int_{t_0}^\infty dt \boldsymbol{E}(\bar{t}-(\tau+\tau_\alpha))\cdot\hat{d}\,|d\,(\boldsymbol{p}-\boldsymbol{A}(\bar{t}-\tau_\alpha))| \tag{14}$$
$$\times e^{i\left[\frac{p^2}{2}+I_p\right](T-\bar{t})}\exp\left\{iA_0(\bar{t}-\tau_\alpha)\sqrt{1+(\alpha\omega)^2}\left(p_x\int_{\bar{t}}^{T_x} dt'\cos(\omega t') + p_y\int_{\bar{t}}^{T_y} dt'\sin(\omega t')\right)\right\}$$

In addition, we assume that the time shift, $\tau_\alpha \sim \alpha$ is small and we can neglect this change in the magnitude of the vector potential and in the value of the ionization dipole matrix element. Changing $\bar{t} \to t$ yields,

$$b(\boldsymbol{p},\tau) = ie^{-i(\int_T^\infty dt' \frac{p^2+A^2}{2} + I_p(T+\alpha))} \int_{t_0}^\infty dt \boldsymbol{E}[t-(\tau+\tau_\alpha)]\cdot\hat{d}\,|d\,(\boldsymbol{p}-\boldsymbol{A}(t))|\, e^{i(\frac{p^2}{2}+I_p)(T-t)}$$

$$\times \exp\left\{ iA_0(t)\sqrt{1+(\alpha\omega)^2}\left(p_x \int_t^{T_x} dt' \cos(\omega t') + p_y \int_t^{T_y} dt' \sin(\omega t') \right) \right\} \tag{15}$$

Comparing Eq. (7) and Eq. (15) shows that the effect of the linear phase of the dipole matrix element is equivalent to shifting the arrival time of the x-ray pulse $E(t)$ and increasing the vector potential by a small factor, $\sqrt{1+(\alpha\omega)^2}$.

B. Dipole Matrix Phase Maps to Streaking Angle

We can also show that the photoionization phase is encoded by the streaking angle by an extension of the isochrone analysis in [2]. We use the same expression for the photoionization dipole matrix element as above in Eq. (9), and the same expression (1) for the photoionization yield in the presence of a circularly polarized streaking field. This gives the following equation for photoionization yield:

$$\begin{aligned} b(\boldsymbol{p},\tau) &= i\int_{t_0}^{\infty} dt \boldsymbol{E}(t-\tau)\cdot\vec{d}(\boldsymbol{p}-\boldsymbol{A}(t))\, e^{-i\Phi(t)} \\ &= i\int_{t_0}^{\infty} dt \boldsymbol{E}(t-\tau)\cdot\left|\vec{d}(\boldsymbol{p}-\boldsymbol{A}(t))\right| e^{-i\alpha[\boldsymbol{p}-\boldsymbol{A}(t)]^2/2} \\ &\qquad \times\exp\left[-\frac{i}{2}\int_t^{\infty} dt' \frac{1}{2}\left[\boldsymbol{p}-\boldsymbol{A}(t')\right]^2 - I_p t\right] \end{aligned}$$

To find the isochrones, we use the stationary point approximation:

$$\begin{aligned} \frac{d}{dt}\left[-\int_t^{\infty} dt'\left(\frac{1}{2}\left(\boldsymbol{p}-\boldsymbol{A}(t')\right)^2\right) - I_p t + \alpha\left(\boldsymbol{p}-\boldsymbol{A}(t)\right)^2/2\right] &= 0 \\ \frac{1}{2}\left(\boldsymbol{p}-\boldsymbol{A}(t_{st})\right)^2 - I_p + \frac{\alpha}{2}\frac{d}{dt}\left[\left(\boldsymbol{p}-\boldsymbol{A}(t)\right)^2\right] &= 0 \\ \frac{1}{2}\left(p^2+A^2(t_{st})-2\boldsymbol{p}\cdot\boldsymbol{A}(t)\right) - I_p + \frac{\alpha}{2}\frac{d}{dt}\left[\left(p^2+A^2(t)-2\boldsymbol{p}\cdot\boldsymbol{A}(t)\right)\right] &= 0 \end{aligned}$$

The streaking field, which is circularly polarized with approximately constant field amplitude in the time period we are interested in, is described by $\boldsymbol{A}(t) = A_0\cos(\omega t)\hat{x} + A_0\sin(\omega t)\hat{y}$. The electron momentum is defined by $\boldsymbol{k} = k\cos\phi\ \hat{x} + k\sin\phi\ \hat{y}$, where ϕ is the emission angle. The dot product $\boldsymbol{k}\cdot\boldsymbol{A}(t) = kA_0\cos(\phi-\omega t)$. This gives,

$$\begin{aligned} \frac{1}{2}\left(p^2+A_0^2-2I_p\right) - kA_0\left[\cos(\phi-\omega t_{st}-\alpha\omega\sin(\phi-\omega t_{st})\right] &= 0 \\ \frac{1}{2}\left(p^2+A_0^2-2I_p\right) - kA_0\sqrt{1+\omega^2\alpha^2}\left[\cos(\phi-\omega t_{st}+\tau_\alpha)\right] &= 0 \end{aligned} \tag{16}$$

In the last line, we use the same identity as before:

$$A\sin x + B\cos x = \sqrt{1+(AB)^2}\sin\left[x+\arctan(A/B)\right]\ .$$

The isochrone now has two shifts: the XUV/IR delay shown in Kazansky et al. [2] derivation, ωt_{st}, and the group delay from the dipole ionzation matrix element, $\tau_\alpha \sim \alpha$. Thus, if we can eliminate the XIR delay contribution we can directly read the EWP group delay from the streaking angle. In the simulation of the main paper, the XIR delay is eliminated by recording the streaking angle for multiple XIR delay values and finding their common offset (angular method). Experimentally, we need to measure the EWP group delay on a single shot basis due to timing jitter inherent to the stochastic nature of XFEL radiation. Rather than systematically varying the XIR delay, we use a reference. This can either be a second ionization state in the same sample or ionization from a second, reference sample mixed with the target sample. The reference and target photolines are produced by the same x-ray pulse, so they share a common global streaking angle. Their difference in streaking angle will give $\tau_a - \tau_r$, where τ_r is the reference's EWP group delay. If we choose a reference photoline that is much higher in energy, for example above 40 eV, and has a clear continuum, then τ_r will be negligible.

II. ON THE EQUIVALENCE OF THE LOPT AND SFA TREATMENTS

In this section, we investigate in detail the relation between the the lowest order perturbation theory (LOPT) treatment and show that, under certain conditions, it is approximately equivalent to the SFA. Using SFA we can

write a general expression for the ionization amplitude of ionization into the state with asymptotic momentum $\boldsymbol{k}$ under the combined action of both XUV and IR fields as [2]

$$\mathcal{M}(\mathbf{k}) = -\frac{i}{2}\int\limits_{-\infty}^{\infty} \langle \boldsymbol{k}|d_x|\phi_0\rangle \mathcal{E}(t) e^{i[\Phi(t) - \omega_X t]}\, dt\ , \tag{17}$$

where $\Phi(t)$ is the phase given by Eq. (2), ω_X and $\mathcal{E}(t)$ are the central frequency and the envelope of the XUV pulse, $\boldsymbol{A}(\tau)$ is the vector potential of the IR field. According to Eq. (17), the effect of the IR field can be described as "dressing" of the final electron state ionized by the XUV pulse. The SFA phase factor accounts for this dressing effect. For simplicity, we assume that IR field is monochromatic, so that its vector potential is of the form specified in the equation 3 above with constant envelope A_0. We can rewrite the SFA phase factor in equation 17 as:

$$e^{i\Phi(t)} = \exp\left\{ i\left[\frac{\boldsymbol{k}^2}{2} + U_p - I_p\right] t - \int\limits_{t}^{\infty} \boldsymbol{k}\cdot\boldsymbol{A}(\tau)\, d\tau \right\}\ , \tag{18}$$

where $U_p = A_0^2/2$ is the ponderomotive energy of an electron in the circularly polarized field given by Eq. (3).

Using the Fourier-Bessel expansion [3], the time integral in Eq. (18) can be expanded as

$$\exp\left\{ -i\int\limits_{t}^{\infty} \boldsymbol{k}\cdot\boldsymbol{A}(\tau)\, d\tau \right\} = \sum_{n=-\infty}^{\infty} J_n\left(\frac{A_0 k}{\omega}\right) e^{in(\omega t+\phi)}\ , \tag{19}$$

where $J_n(z)$ is the Bessel function of order n. One thus represents the amplitude (17) as a sum of the contributions $\mathcal{M}_n(\mathbf{k})$ with different n. Every term

$$\mathcal{M}_n(\mathbf{k}) = -\frac{i}{2} J_n\left(\frac{A_0 k}{\omega}\right) e^{in\phi} \int\limits_{-\infty}^{\infty} \langle \boldsymbol{k}|d_x|\phi_0\rangle \mathcal{E}(t) e^{i\left(\frac{\boldsymbol{k}^2}{2} + U_p - \omega_x + n\omega - I_p\right) t}\, dt \tag{20}$$

can be naturally interpreted as an amplitude of absorption of an XUV photon accompanied by an absorption (for $n < 0$) or emission (for $n > 0$) of n IR photons.

For a weak IR field under consideration, we are interested only in the terms with $n = \pm 1$ corresponding to absorption and emission of an IR photon. Furthermore, by using the small argument approximation for the Bessel function $J_n(z) \propto z$ and neglecting the ponderomotive energy (which is permissible for the weak IR field), Eq. (20) reduces to an expression similar to the second order LOPT. Most importantly, the angular ansatz that we employed in our fitting procedure is identical in SFA and LOPT.

---

[1] D. Kiesewetter, R. R. Jones, A. Camper, S. B. Schoun, P. Agostini, and L. F. DiMauro, *Probing electronic binding potentials with attosecond photoelectron wavepackets*, Nature Physics **14**, 68 (2018).

[2] A. K. Kazansky, A. V. Bozhevolnov, I. P. Sazhina, and N. M. Kabachnik, *Interference effects in angular streaking with a rotating terahertz field*, Phys. Rev. A **93**, 013407 (2016).

[3] S. V. Popruzhenko, *Keldysh theory of strong field ionization: history, applications, difficulties and perspectives*, J. Phys. B **47**(20), 204001 (2014).